A Synthesis of geometry effect on brittle fracture

S.M.J. Razavi[a], M.R. Ayatollahi[b], F. Berto[a]

[a] *Department of Mechanical and Industrial Engineering, Norwegian University of Science and Technology (NTNU), Richard Birkelands vei 2b, 7491, Trondheim, Norway.*

[b] *Fatigue and Fracture Lab., Centre of Excellence in Experimental Solid Mechanic and Dynamics, School of Mechanical Engineering, Iran University of Science and Technology, Narmak, 16846, Tehran, Iran.*

Abstract

There are numerous analytical solutions in order to take into account the geometry effect on the fracture toughness and the fracture load of the cracked specimens. However, due to the complexities of the mentioned criteria it is practical to have an engineering method which can be used for fracture prediction in cracked samples of various shapes and loading conditions. In this paper, the fracture behavior of five different testing samples made of polymethylmethacrylate (PMMA) has been studied using an energy based criterion namely the Average Strain Energy Density (ASED) criterion. According to the formulation of the ASED criterion, all the stress terms around the crack tip were taken into account and the brittle fracture of different PMMA samples with various geometry constraints were well predicted.

Keywords: Average strain energy density criterion; Brittle fracture; T-stress; Finite element analysis

Nomenclature

a	crack length
B	biaxiality ratio
E	elastic modulus
h_1	minor height of cracked specimen
h_2	major height of cracked specimen
K_{I}	mode-I stress intensity factor
K_{Ic}	mode-I fracture toughness
F	applied load in finite element analysis
F_{c}	fracture load
r_{c}	critical distance
T	T-stress
W	width of cracked specimen
σ_t	ultimate strength
v	Poisson's ratio
ASED	Average strain energy density criterion
ASTM	American society of testing materials
CT	compact tension specimen
DCB	double cantilever beam specimen
TDCB	tapered double cantilever beam specimen
GMTS	generalized maximum tangential stress criterion
GSED	generalized minimum strain energy density criterion
LEFM	linear elastic fracture mechanics
MTS	maximum tangential stress criterion
PMMA	polymethylmethacrylate

SED	strain energy density criterion
SIF	stress intensity factor
$\bar{W}$	average strain energy density
W_c	critical strain energy density

1. Introduction

Brittle fracture is the dominant failure mechanism in a wide range of brittle and quasi-brittle materials. Hence, failure load assessment is an important task for numerous practical applications of brittle materials such as rocks, concretes, ceramics and polymers. The majority of available researches in this field are related to the failure criteria based on singular terms of stress at the vicinity of the crack tip. Considering the pure mode I loading, cracks can be deviated from the original crack plane due to the presence of large values of higher order terms of stresses. In this case, several researchers have shown that the fracture toughness of the materials is considerably different from the results obtain from the standard testing samples such as Compact Tension (CT) and these differences are influenced by the shape of the tested specimen [1-12].

In this case the available fracture criteria which are based on only the singular terms of stress (i.e. stress intensity factor, SIF) fail to predict the onset of the fracture [1-4]. One possibility is to include the higher order terms (such as T-stress) contribution in the fracture criteria by reformulating the previous models based on SIFs. Various fracture criteria have been proposed based on the leading terms of series expansion governed by the SIFs combined with the T-stress. It has been reported that these two-parameter fracture criteria provide more reliable fracture assessments [13–16]. Among the various two-parameter fracture criteria, the generalized maximum tangential stress (GMTS) and generalized strain energy density

(GSED) criteria are mostly used for brittle fracture of cracked specimens [10,11]. The GMTS and GSED criteria are modified versions of maximum tangential stress (MTS) [17] and strain energy density (SED) [18,19] criteria by considering the effect of T-stress in the closed form formulations. Although these failure criteria provide better approximation of the fracture behavior, they have more complex formulations compared to the previous models based on SIF.

Lazzarin and Zambardi [20,21] presented the ASED criterion by improving the SED criterion and considering a control volume instead of a critical distance. According to the ASED criterion, brittle fracture occurs when the averaged strain energy density over a control volume is equal to a critical value which is a function of material properties of the material. By using a control volume around the crack tip and obtaining the strain energy densities, all terms of Williams's series can be considered in calculations leading to more accurate results. Although successful ability of the ASED criterion has been reported in several researches for various loading conditions in different engineering materials (such as rocks, graphite, polymers, metals, and etc. [22-30]) and different practical applications (such as welded joints in constructional industries [31] and roller in metal forming industries [32]), the validity of this criterion has not yet been examined for different geometries of cracked specimens. Hence, the main aim of the present research is to investigate mode I brittle fracture in PMMA testing samples of five different geometries. For this aim, the experimental fracture results of PMMA specimens reported in a recently published article of the current authors (see Ref. [11]) are assessed using the ASED criterion. It has been shown that very good agreement exists between the experimental results and the theoretical findings.

2. Experiments

Fig. 1 illustrates the geometry of five different specimens used for conducting the fracture tests, namely CT, two types of double cantilever beam (i.e. DCB^1, DCB^2) and two types of tapered double cantilever beam (i.e. $TDCB^1$, $TDCB^2$). Due to different geometric constraints in these specimens, they can provide a wide range of positive *T*-stress. Samples were cut from a PMMA sheet of 10 mm thick. The geometrical dimensions of the test samples are provided in Table 1. The initial notch in the samples was created using a 0.2 mm thick strip saw blade. Then, a razor blade was pressed on the notch tip to create a sharp pre-crack. The final crack length for all the cases was equal to $a/W = 0.5$.

Table 1. The geometrical dimensions of the test samples [11] (all dimensions in mm).

Sample type	Width, W	Minor height, h_1	Major height, h_2	Pre-crack length, a
CT	30	30	30	15
DCB^1	90	30	30	45
DCB^2	150	30	30	75
$TDCB^1$	90	30	90	45
$TDCB^2$	150	30	90	75

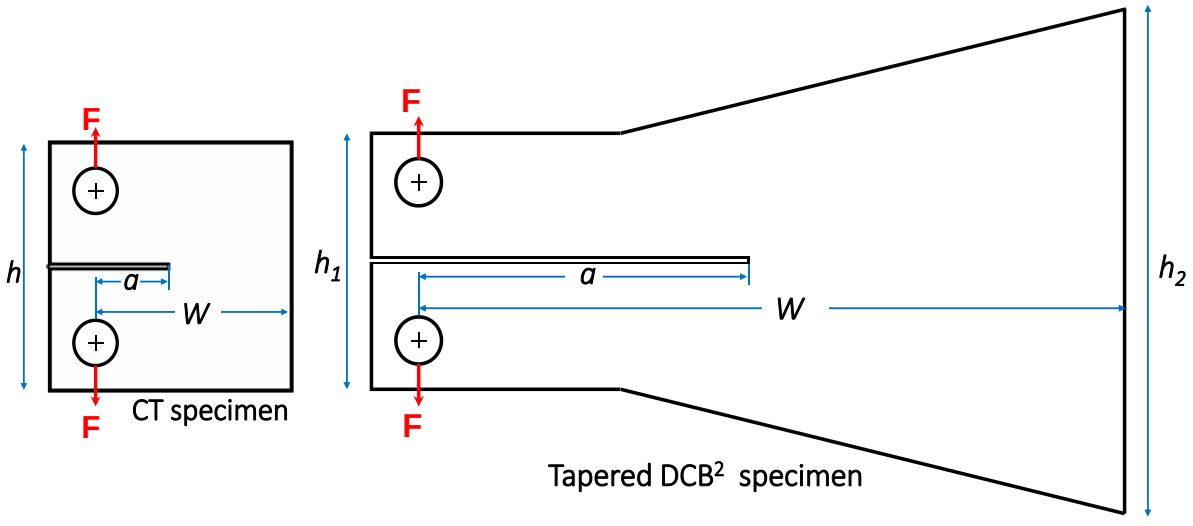

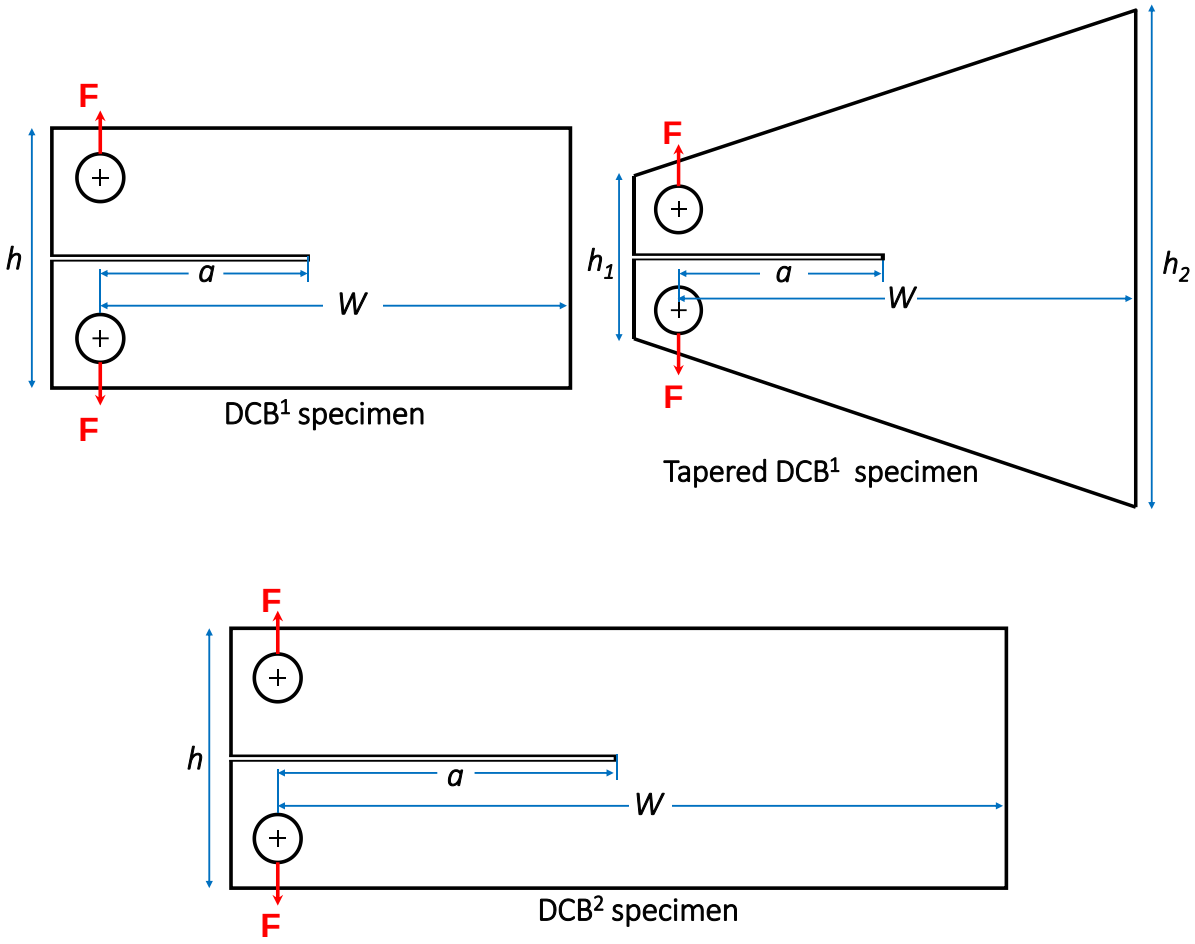

Fig. 1. Schematic view of specimen geometries [11].

A series of standard tensile tests were conducted according to ASTM D638 to obtain the elastic modulus E and the ultimate tensile strength σ_t of PMMA. Based on earlier study [11, 33] elastic modulus, ultimate tensile strength and Poisson's ratio were obtained as E = 2.9 GPa, σ_t = 55 MPa and ν = 0.35. Additionally, a constant displacement rate of 0.1 mm/min was applied to the fracture test samples and the load-displacement curves were exported for each test. According to the brittle behavior of PMMA in room temperature, all the load-displacement curves had a linear trend followed by sudden failure under critical load. The failure load of CT sample was then used in finite element analyses to obtain the fracture

toughness. In the following sections, the obtained fracture loads are estimated theoretically using the ASED criterion.

3. Theoretical background of ASED criterion

In this research, a strain energy density-based criterion namely the ASED is described and used for fracture load prediction of different test samples under pure mode I loading conditions. According to the ASED criterion, when the mean value of strain energy density over a control volume, $\overline{W}$ is equal to a critical value $W_{c,}$ the pre-cracked sample will fail. The critical strain energy density, W_c is a material property which is independent from the geometry of cracked specimen [20]. The radius of control volume depends on the fracture toughness (K_{Ic}) and the ultimate tensile strength (σ_t) of the materials under static loads.

For the case of cracked components, the control volume is a circle of radius r_c centered at the crack tip (see Fig. 2). Due to the relatively large thickness of the test samples compared to other dimensions, plane strain condition was used in the analysis. Dealing with cracked components under plane-strain condition, the control volume size, r_c, can be calculated using the following expression [34]:

$$r_c = \frac{(1+\nu)(5-8\nu)}{4\pi}\left(\frac{K_{Ic}}{\sigma_t}\right)^2 \tag{1}$$

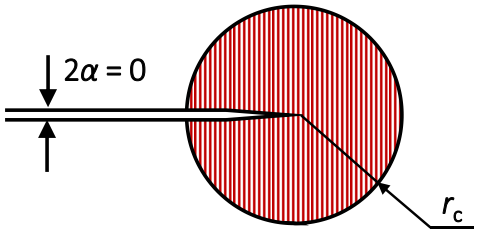

Fig. 2. Schematic view of the control volume around the crack tip.

Lazzarin et al. [20,21] proposed a formula to calculate the average strain energy density using SIFs, however, this formulation neglects the effect of higher order terms of stress in front of the crack tip. According to their research, elastic deformation energy averaged on the control volume turns out to be [20,21]:

$$\bar{W} = \frac{I_1}{4E\,\lambda_1(\pi-\alpha)} \times \left(\frac{K_I}{r_c^{(1-\lambda_1)}} \right)^2 \tag{2}$$

where I_1 is the mode I geometric constant which is a function of the notch geometry and the Poisson's ratio. Additionally, λ_1 is Williams' mode I eigenvalue and K_I is the mode I SIF. Dealing with the specific case of a cracked sample (i.e. 2α = 0), the mode I geometric constant and mode I eigenvalue are equal to I_1 = 0.7425 and λ_1 = 0.5. As a result, the mean strain energy density in the control volume around the crack tip can be obtained using Eq. (3).

$$\bar{W} = (0.11817)\frac{K_I^2}{Er_c} \tag{3}$$

On the other hand, to avoid any simplifications, the strain energy density values were also directly obtained from the finite element analysis in this paper and the results were compared with those obtained from Eq. (3).

At the onset of fracture, the average strain energy density, $\bar{W}$ reaches its critical value, W_c. The critical strain energy density, W_c can be obtained as a function of σ_t and E [20,21]:

$$W_c = \frac{\sigma_t^2}{2E} \tag{4}$$

The critical strain energy density value is considered to be constant for different sample geometries. Considering the average strain energy density value $\bar{W}$ to be equal to the critical

value W_c, the fracture load of the cracked specimens can be obtained. Thus, using a simple proportion between the applied load F in finite element analyses and the square root values of averaged strain energy density, the theoretical fracture loads (F_{ASED}) can be calculated as given below

$$F_{ASED}/F = \sqrt{W_c/\bar{W}} \tag{5}$$

In order to have a quantitative parameter to evaluate the geometry effect, the biaxiality ratio, B was introduced to show the ratio of the T-stress relative to the SIF (see Eq. 6) [35]. Higher values of biaxiality ratio demonstrate higher geometry constraints in the samples resulting to lower fracture toughness. Additionally, it has been reported by Ayatollahi et al. [11] that higher values of B increase the probability of crack kinking out of its initial direction.

$$B = \frac{T\sqrt{\pi a}}{K_I} \tag{6}$$

4. Finite element model

In order to obtain the SIF, T-stress and strain energy density, two dimensional finite element models of the tests samples were analyzed. An interaction integral method built in finite element software was used in order to directly obtain the SIFs and the T-stress [36, 37]. A typical mesh pattern generated for modeling one of the test samples is shown in Fig. 3. Two dimensional stress analyses were conducted using the elastic properties of PMMA as presented in Section 2. Due to the relatively large value of thickness of the tested samples in comparison with the other dimensions, plane strain elements were used for finite element analyses. The model was meshed using iso-parametric 8-node quadrilateral elements.

Although ASED calculations doesn't require fine elements, fine singular elements have been used in the first ring of elements surrounding the crack tip to produce the square root singularity of the stress field around the crack tip resulting in more accurate SIF and T-stress values. By considering different sizes of elements in the control volume, a mesh convergence study was undertaken on the SIF values to ensure that proper element sizes were used in the finite element analyses.

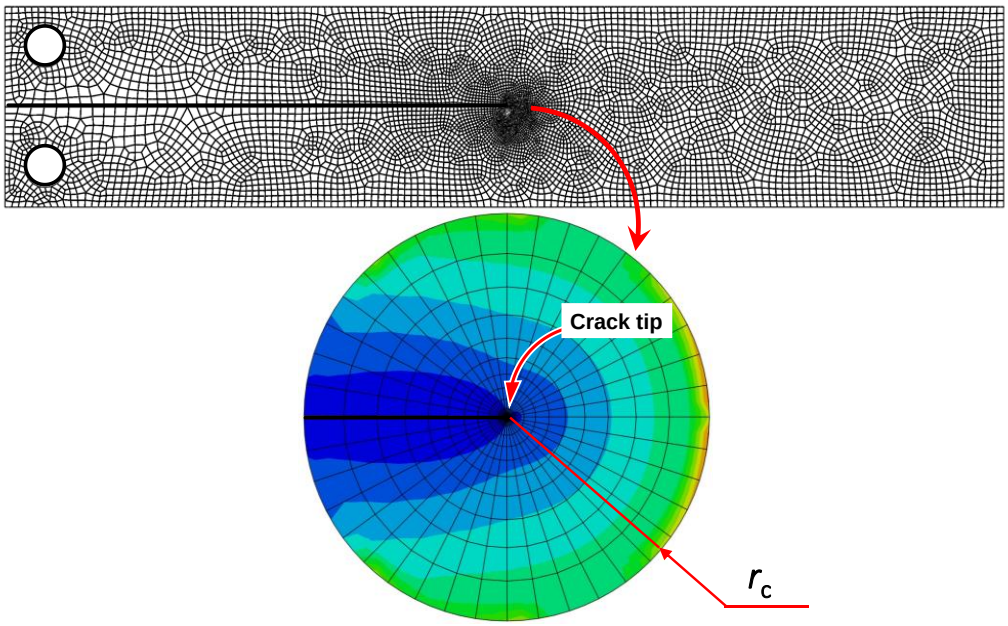

Fig. 3. A typical mesh pattern used for finite element analysis and exploring the variation of strain energy inside the control volume for DCB[1] specimen.

5. Results and discussion

According to the experimental data on the CT specimens, a fracture toughness of K_{Ic} = 44.27 $\text{MPa}\sqrt{\text{mm}}$ was obtained from CT specimens which was used in critical strain energy density calculations. By substituting fracture toughness (K_{Ic} = 44.27 $\text{MPa}\sqrt{\text{mm}}$) and tensile strength ($\sigma_t$ = 55 MPa) of PMMA into Eq. (1), the calculated value of critical radius, r_c was found to

be 0.153 mm. In order to obtain the mean strain energy density in the control volume and the crack tip parameters, a unit concentrated force was applied to the loading pins of the finite element models (i.e. F = 1 N). The critical strain energy density was equal to W_c = 0.522 mJ/mm^3. The theoretical ASED predictions were obtained using Eq. (5).

Table 2 presents the finite element results of SIF and T-stress corresponding to the unit applied load in finite element model and the mean strain energy density values obtained using Eq. (3) in addition to the theoretical ASED predictions based on Eq. (3). Additionally, the mean strain energy density values corresponding to the unit applied load in finite element analysis and the theoretical ASED predictions based on the finite element analysis are presented in Table 3. A comparison between the experimental fracture loads and the ASED predictions based on finite element analysis is presented in Fig. 4.

According to the ASED predictions based on the constant value of W_c = 0.522 mJ/mm^3 for different specimen geometries, maximum discrepancies of 8% and 4% were obtained for the predictions based on Eq. (3) and finite element results, respectively. Although both ASED predictions are quite acceptable, however, application of finite element software for ASED calculations results in more precise predictions with almost half discrepancies compared to Eq. (3) which is based on the singular term of Williams' series.

Table. 2. Outline of numerical results for the test specimens

(The numerical values of $\overline{W}$ are obtained using Eq. (3) based on K_I)

Specimen type	K_I [MPa$\sqrt{\text{mm}}$]	T-stress [MPa]	B	$\overline{W}\|_{\text{theor.}}$ [mJ/mm^3]	Average fracture load F_{exp} [N] (Experiments)	Fracture load $F_{\text{theor.}}$ [N] (prediction based on K_I)	Discrepancy$\|_{\text{theor.}}$ (%)
CT	0.14	0	0.51	5.11e-6	319 (4%)*	319	0
DCB[1]	0.29	6.79e-3	1.14	2.28e-5	141 (4%)	151	-7
DCB[2]	0.47	6.29e-3	2.15	5.92e-5	87 (4%)	94	-8
TDCB[1]	0.12	6.01e-3	1.14	3.83e-6	367 (9%)	369	-1

TDCB[2]	0.24	5.92e-3	2.06	1.48e-5	175 (9%)	188	-7

* Standard deviation

Table. 3. Outline of numerical results for the test specimens

(The numerical values of $\bar{W}$ are obtained directly from the finite element analysis)

Specimen type	K_I [$MPa\sqrt{mm}$]	T-stress [MPa]	B	$\bar{W}\|_{FEM}$ [mJ/mm^3]	Average fracture load F_{exp} [N] (Experiments)	Fracture load F_{FEM} [N] (ASED prediction)	Discrepancy$\|_{FEM}$ (%)
CT	0.14	0	0.51	5.12e-6	319 (4%)*	319	0
DCB[1]	0.29	6.79e-3	1.14	2.42e-5	141 (4%)	147	-4
DCB[2]	0.47	6.29e-3	2.15	6.38e-5	87 (4%)	90	-4
TDCB[1]	0.12	6.01e-3	1.14	3.95e-6	367 (9%)	363	-1
TDCB[2]	0.24	5.92e-3	2.06	1.60e-5	175 (9%)	181	-3

* Standard deviation

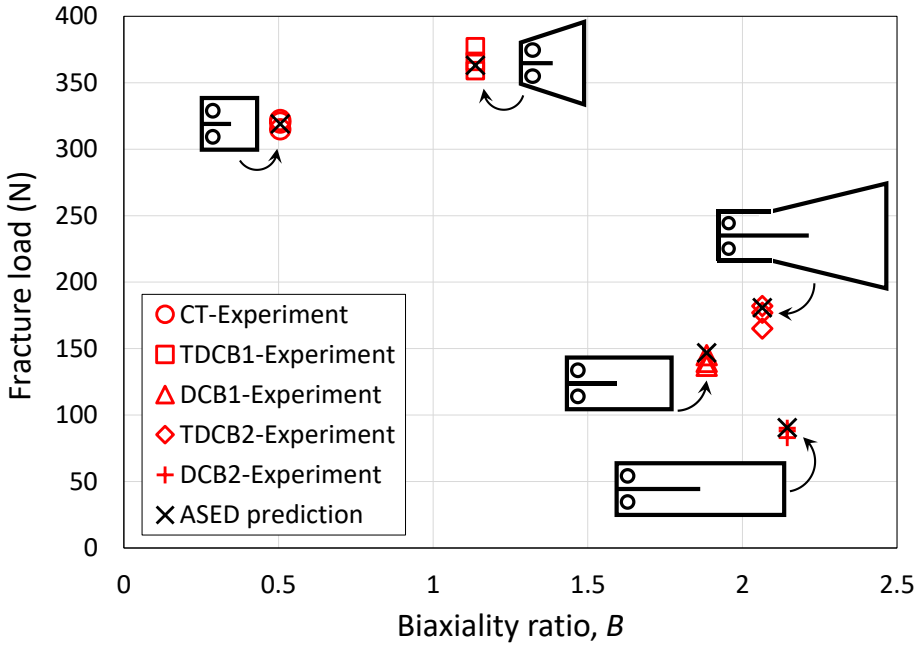

Fig. 4. Comparative results of the experimental fracture loads and ASED predictions.

A comprehensive synthesis expressed in terms of the square root of the average strain energy density normalized by its critical value, W_c, as a function of the biaxiality ratio, B is illustrated in Fig. 5. The parameter $(W/W_c)^{0.5}$ is proportional to the fracture loads of the tested samples. According to the ASED synthesis, it is confirmed that the chosen control volume is capable of considering the geometry effect on the fracture behaviour of PMMA samples. According to Fig. 5, it is obvious that the majority of fracture load predictions are well inside the scatter band ranging between ± 10% with considerable number of the results falling inside the scatter ranging between ± 5%.

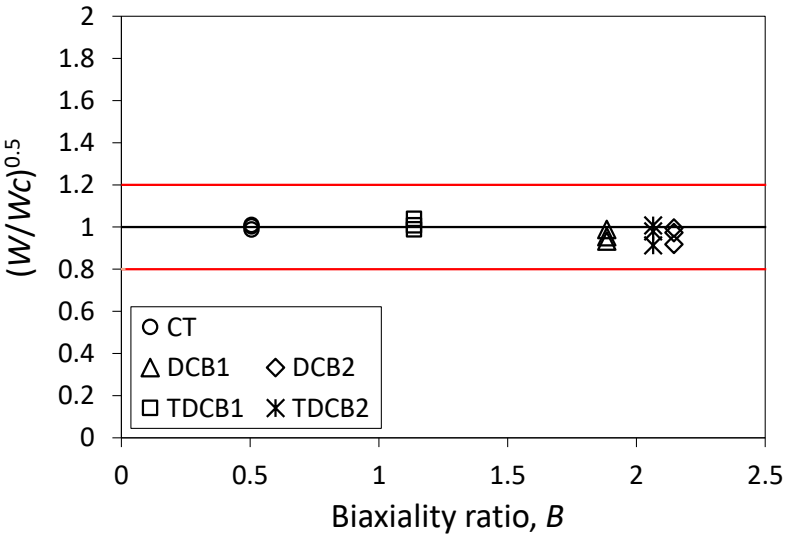

Fig. 5. Synthesis of fracture data in terms of normalized ASED.

It is worth mentioning that the fracture load of brittle materials are commonly obtained using single parameter fracture criteria which are based on the critical SIF corresponding to the fracture load of the material. It was shown in this paper that considering the higher order terms of Williams' series in ASED calculations leads to more accurate fracture load predictions. Hence, the single parameter fracture criteria can provide reliable fracture predictions only for limited range of geometry.

In general, the ASED criterion can be used by engineers and scientists to predict the onset of fracture in complex pre-cracked parts without requiring costly and time-consuming experiments. On the other hand, the simple ASED criterion can provide very good fracture prediction compared to the available complex double parameter fracture criteria (based on SIF and T-stress). The presented fracture predictions in this research confirmed the accuracy and practical ability of ASED criterion for evaluating the fracture behavior of various cracked samples subjected to mode I loading with a very limited discrepancy.

Ayatollahi et al. [11] reported that for materials with high critical distance r_c, e.g. rock materials, the *T*-stress becomes no longer negligible when calculating SED inside the control

volume. Hence, the *T*-stress can play an important role in fracture behavior of materials possessing larger critical radii. In that case, the importance of using a fracture criterion, which counts for higher order terms, would be even more important. Hence the fracture behavior of three different rocks (i.e. Harsin marble, Johnstone, South Korean Yeosan) were assessed both with single parameter fracture model (Eq. 3) and ASED criterion. The material properties of the mentioned rocks are presented in Table 4. According to Table 4, it can be observed that the critical radius of the presented rock materials are one order of magnitude bigger than that of PMMA.

Table. 4. Material properties of the investigated rocks.

Material property	Harsin marble [38]	Johnstone [40-42]	South Korean Yeosan [43]
Elastic modulus, E [GPa]	70 [39]	0.20	48 [44]
Poisson's ratio, v	0.28 [39]	0.30	0.31 [44]
Fracture toughness, K_{Ic} [$MPa\sqrt{mm}$]	31.62	2.20	27.50
tensile strength, σ_t [MPa]	7.20	0.44	6 [45,46]
Critical radius, r_c [mm]	5.42	6.72	5.52

The fracture load predictions based on ASED method and single parameter model are presented in Tables 5 to 7 respectively for Harsin marble, Johnstone, South Korean Yeosan rocks.

Table. 5. Outline of numerical results for the fracture of Harsin marble rock.

Specimen type	$\bar{W}\|_{theor.}$ [mJ/mm^3]	$\bar{W}\|_{FEM}$ [mJ/mm^3]	Fracture load $F_{theor.}$ [N] (prediction based on K_I)	Fracture load F_{FEM} [N] (ASED prediction)	Δ* (%)
CT	5.98e-9	5.37e-9	248.82	262.65	5
DCB[1]	2.67e-8	4.16e-8	117.78	94.35	-25
DCB[2]	6.92e-8	1.24e-7	73.13	54.62	-34
TDCB[1]	4.48e-9	6.45e-9	287.38	239.57	-20

TDCB[2]	1.73e-8	3.73e-8	146.31	99.64	-47

* $\Delta = (F_{FEM} - F_{theor.}) / F_{FEM} \times 100$

Table. 6. Outline of numerical results for the fracture of Johnstone rock.

Specimen type	$\bar{W}\|_{theor.}$ [mJ/mm^3]	$\bar{W}\|_{FEM}$ [mJ/mm^3]	Fracture load $F_{theor.}$ [N] (prediction based on K_I)	Fracture load F_{FEM} [N] (ASED prediction)	Δ (%)
CT	1.69e-6	1.37e-6	16.93	18.78	10
DCB[1]	7.53e-6	1.11e-5	8.02	6.61	-21
DCB[2]	1.95e-5	3.36e-5	4.98	3.79	-31
TDCB[1]	1.27e-6	1.73e-6	19.56	16.74	-17
TDCB[2]	4.88e-6	1.04e-5	9.96	6.81	-46

Table. 7. Outline of numerical results for the fracture of South Korean Yeosan rock.

Specimen type	$\bar{W}\|_{theor.}$ [mJ/mm^3]	$\bar{W}\|_{FEM}$ [mJ/mm^3]	Fracture load $F_{theor.}$ [N] (prediction based on K_I)	Fracture load F_{FEM} [N] (ASED prediction)	Δ (%)
CT	8.57E-09	7.23E-09	209.18	227.82	8
DCB[1]	3.82E-08	5.60E-08	99.02	81.83	-21
DCB[2]	9.92E-08	1.68E-07	61.48	47.27	-30
TDCB[1]	6.42E-09	8.56E-09	241.61	209.35	-15
TDCB[2]	2.48E-08	5.02E-08	123.01	86.41	-42

Although the current methodology was presented for a brittle material (i.e. PMMA), however, the same method can be employed to predict the ductile failure of cracked and notched components by equating the real ductile material with a brittle material having a virtual ultimate strength. Using the ASED method, the failure loads of the ductile notched components were successfully predicted without requiring time-consuming and complex

elastic-plastic finite element analyses [26, 27]. The same technique can be used in order to assess the geometry effect of ductile materials.

6. Conclusions

In this paper, the average strain energy density (ASED) criterion was used to assess the fracture load of five different test sample geometries under mode I. Application of classical fracture models for the cases with high geometry constraints results in higher discrepancies of the predictions, which can be a result of neglecting the higher order terms in these models. The ASED criterion that includes all terms of Williams's series could provide considerably improved predictions for the experimental data obtained from PMMA specimens of different shapes. The same methodology can be used to estimate the fracture load of other brittle and quasi-brittle materials.

References

[1] S.G. Larsson, A.J. Carlsson, Influence of non-singular stress and specimen geometry on small-scale yielding at each tip in elastic-plastic materials, Journal of Physics and solids 21 (1973) 263–277.

[2] J.R. Rice, Limitations to the small scale yielding for crack-tip plasticity, Journal of Mechanic of Physics and solids 22 (1974) 17–26.

[3] C. Betegon, J.W. Hancock, Two-parameter characterization of elastic-plastic crack-tip fields, Journal of Applied Mechanics 58 (1991) 104–110.

[4] Z.Z. Du, J.W. Hancock, The effect of non-singular stresses on crack tip constraint, Journal of Mechanic of Physics and solids 39 (1991) 555–567.

[5] M. Moattari, I. Sattari-Far, Modification of fracture toughness Master Curve considering the crack-tip Q-constraint, Theoretical and Applied Fracture Mechanics 90 (2017) 43-52.

[6] B. Kumar, S. Chitsiriphanit, C.T. Sun, Significance of K-dominance zone size and nonsingular stress field in brittle fracture, Engineering Fracture Mechanics 78 (2011) 2042–2051.

[7] C.T. Sun, H. Qian, Brittle fracture beyond the stress intensity factor, Journal of Mechanics of Materials and Structures 4 (2009) 743–753.

[8] S. Liu, Y.J. Chao, Variation of fracture toughness with constraint, International Journal of Fracture 124 (2003) 113–117.

[9] Y.J. Chao, S. Liu, B.J. Broviak, Brittle fracture: variation of fracture toughness with constraint and crack curving under mode I conditions, Experimental Mechanics 41 (2001) 232–241.

[10] M.R. Ayatollahi, S.M.J. Razavi, M. Rashidi Moghaddam, F. Berto, Mode I fracture analysis of Polymethylmetacrylate using modified energy—based models, Physical Mesomechanics 18(5) (2015) 53-62.

[11] M.R. Ayatollahi, M. Rashidi Moghaddam, S.M.J. Razavi, F. Berto, Geometry effects on fracture trajectory of PMMA samples under pure mode-I loading, Engineering Fracture Mechanics 163 (2016) 449–461.

[12] M. Rashidi Moghaddam, M.R. Ayatollahi, S.M.J. Razavi, F. Berto, Mode II Brittle Fracture Assessment Using an Energy Based Criterion, Physical Mesomechanics 20(2) (2017) 142–148.

[13] D.J. Smith, M.R. Ayatollahi, M.J. Pavier, The role of T-stress in brittle fracture for linear elastic materials under mixed-mode loading, Fatigue and Fracture of Engineering Materials and Structures 24 (2001) 137–150.

[14] Y.F. Li, S.M. Dong, W. Hua, T-stress for central cracked Brazilian disk subjected to compression, Yantu Lixue/Rock and Soil Mechanics 37(11) (2016) 3191-3196.

[15] L. Malikova, V. Vesely, S. Seitl, Crack propagation direction in a mixed mode geometry estimated via multi-parameter fracture criteria, International Journal of Fatigue 89 (2015) 99-107.

[16] L. Malikova, Multi-parameter fracture criteria for the estimation of crack propagation direction applied to a mixed-mode geometry, Engineering Fracture Mechanics 143 (2015) 32-46.

[17] F. Erdogan, G.C. Sih, On the crack extension in plates under plane loading and transverse shear, Journal of Basic Engineering 85 (D) (1963) 519-527.

[18] G.C. Sih, Strain-energy-density factor applied to mixed mode crack problems, International Journal of Fracture 10 (1974) 305–321.

[19] G.C. Sih, Some basic problems in fracture mechanics and new concepts, Engineering Fracture Mechanics 5 (1973) 365–377.

[20] P. Lazzarin, R. Zambardi, A finite-volume-energy based approach to predict the static and fatigue behaviour of components with sharp V-shaped notches, International Journal of Fracture 112 (2001) 275–298.

[21] P. Lazzarin, F. Berto, Some expressions for the strain energy in a finite volume surrounding the root of blunt V-notches, International Journal of Fracture 135 (2005) 161–185.

[22] F. Berto, A. Campagnolo, P. Gallo, Brittle Failure of Graphite Weakened by V-Notches: A Review of Some Recent Results Under Different Loading Modes, Strength of Materials, 47(3) (2015) 488–506.

[23] M.R. Ayatollahi, F. Berto, A. Campagnolo, P. Gallo, K. Tang, Review of local strain energy density theory for the fracture assessment of V-notches under mixed mode loading, Engineering Solid Mechanics, 5(2) (2017) 113-132.

[24] P. Gallo, F. Berto, Advanced Materials for Applications at High Temperature: Fatigue Assessment by Means of Local Strain Energy Density, Advanced Engineering Materials, 18(12) (2016) 2010–2017.

[25] P. Gallo, T. Sumigawa, T. Kitamura, F. Berto, Evaluation of the strain energy density control volume for a nanoscale singular stress field, Fatigue and Fracture of Engineering Materials and Structures, 39(12) (2016) 1557–1564.

[26] A. Torabi, F. Berto, S.M.J. Razavi, Ductile failure prediction of thin notched aluminum plates subjected to combined tension-shear loading, Theoretical and Applied Fracture Mechanics (in press) (DOI: 10.1016/j.tafmec.2017.05.003)

[27] A. Torabi, F. Berto, S.M.J. Razavi, Tensile failure prediction of U-notched plates under moderate-scale and large-scale yielding regimes, Theoretical and Applied Fracture Mechanics (in press) (DOI: 10.1016/j.tafmec.2017.07.009)

[28] S.M.J. Razavi, F. Berto, M.R. Aliha, Application of an average strain energy density criterion to obtain the fracture load of granite cracked asymmetric four-point bend specimens under mixed mode loading conditions, Theoretical and Applied Fracture Mechanics (in press) (DOI: 10.1016/j.tafmec.2017.07.004)

[29] S.M.J. Razavi, P. Ferro, F. Berto, J. Torgersen, Fatigue strength of blunt V-notched specimens produced by Selective Laser Melting of Ti-6Al-4V, Theoretical and Applied Fracture Mechanics (in press). (DOI: 10.1016/j.tafmec.2017.06.021)

[30] M.R.M. Aliha, F. Berto, A. Mousavi, S.M.J. Razavi, On the applicability of ASED criterion for predicting mixed mode I+II fracture toughness results of a rock material, Theoretical and Applied Fracture Mechanics (in press) (DOI: 10.1016/j.tafmec.2017.07.022)

[31] P. Lazzarin, F. Berto, M. Zappalorto, Rapid calculations of notch stress intensity factors based on averaged strain energy density from coarse meshes: Theoretical bases and applications, International Journal of Fatigue 32 (2010) 1559–1567.

[32] F. Berto, A. Campagnolo, F. Chebat, M. Cincera, M. Santini, Fatigue strength of steel rollers with failure occurring at the weld root based on the local strain energy values: modelling and fatigue assessment, International Journal of Fatigue 82 (2016) 643-657.

[33] M.R. Ayatollahi, M.R.M. Aliha and H. Saghafi, An improved semi-circular bend specimen for investigating mixed mode brittle fracture, Engineering Fracture Mechanics 78 (1) (2011) 110-123.

[34] Z. Yosibash, A. Bussiba, I. Gilad, Failure criteria for brittle elastic materials, International Journal of Fracture 125 (2004) 307–33

[35] P.S. Leevers, J.C. Radon, Inherent stress biaxiality stresses in various fracture specimen geometries, International Journal of Fracture 19 (1982) 311–325.

[36] C.F. Shih, R.J. Asaro, Elastic-Plastic Analysis of Cracks on Bimaterial Interfaces: Part I—Small Scale Yielding, Journal of Applied Mechanics (1988) 299–316. (DOI: doi:10.1115/1.3173676)

[37] Smith M. ABAQUS/Standard User's Manual, Version 6.9. Providence, RI: Simulia, 2009.

[38] M.R.M. Aliha, M.R. Ayatollahi, Mixed mode I/II brittle fracture evaluation of marble using SCB specimen, Procedia Engineering 10 (2011) 311–318.

[39] B.N. Whittaker, R.N. Singh, G.X. Sun, Rock fracture mechanics principles, design and applications. Elsevier, Amsterdam (1992).

[40] I.L. Lim, I.W. Johnston, S.K. Choi, J.N. Boland, Fracture testing of a soft rock with semi-circular specimens under three point bending. Part 1—mode I, International Journal of Rock Mechanics and Mining Sciences & Geomechanics Abstracts 31(3) (1994) 185–197.

[41] I.L. Lim, I.W. Johnston, S.K. Choi, J.N. Boland, Fracture testing of a soft rock with semi-circular specimens under three-point bending. Part 2—mixed mode, International Journal of Rock Mechanics and Mining Sciences & Geomechanics Abstracts 31(3) (1994) 199–212.

[42] M. Rashidi Moghaddam, M.R. Ayatollahi, F. Berto, Rock Fracture Toughness Under Mode II Loading: A Theoretical Model Based on Local Strain Energy Density, Rock Mechanics and Rock Engineering (DOI 10.1007/s00603-017-1319-7)

[43] S.H. Chang, C.I. Lee, S. Jeon, Measurement of rock fracture toughness under modes I and II and mixed-mode conditions by using disk-type specimen, Engineering Geology 66(1-2) (2002) 79–97.

[44] H.S. Lee, Y.J. Park, T.F. Cho, K.H. You, Influence of asperity degradation on the mechanical behavior of rough rock joints under cyclic shear loading, International Journal of Rock Mechanics and Mining Sciences 38 (2001) 967–980.

[45] P.B. Attewell, I.W. Farmer, Principles of engineering geology. Chapman and Hall, London (1976).

[46] G. Hua, Rock cutting using fracture mechanics principles, PhD Dissertation, University of Wollongong (1990).